

Robustifying ℓ_∞ Adversarial Training to the Union of Perturbation Models

Ameya D. Patil, Michael Tuttle, Alexander G. Schwing, and Naresh R. Shanbhag

University of Illinois at Urbana-Champaign
Urbana, IL 61801

{adpatil2,mtuttle3,aschwing,shanbhag}@illinois.edu

Abstract

Classical adversarial training (AT) frameworks are designed to achieve high adversarial accuracy against a single attack type, typically ℓ_∞ norm-bounded perturbations. Recent extensions in AT have focused on defending against the union of multiple perturbations but this benefit is obtained at the expense of a significant (up to $10\times$) increase in training complexity over single-attack ℓ_∞ AT. In this work, we expand the capabilities of widely popular single-attack ℓ_∞ AT frameworks to provide robustness to the union of $(\ell_\infty, \ell_2, \ell_1)$ perturbations while preserving their training efficiency. Our technique, referred to as **Shaped Noise Augmented Processing (SNAP)**, exploits a well-established byproduct of single-attack AT frameworks – the reduction in the curvature of the decision boundary of networks. SNAP prepends a given deep net with a shaped noise augmentation layer whose distribution is learned along with network parameters using any standard single-attack AT. As a result, SNAP enhances adversarial accuracy of ResNet-18 on CIFAR-10 against the union of $(\ell_\infty, \ell_2, \ell_1)$ perturbations by 14%-to-20% for four state-of-the-art (SOTA) single-attack ℓ_∞ AT frameworks, and, for the first time, establishes a benchmark for ResNet-50 and ResNet-101 on ImageNet.

1 Introduction

Today *adversarial training* (AT) provides state-of-the-art (SOTA) empirical defense against adversarial perturbations. For this, adversarial perturbations are used during training to optimize a *robust* loss function [22, 46, 35, 40]. Early AT frameworks [22, 46] were $7\times$ -to- $10\times$ more computationally demanding than vanilla training. More recent works [35, 40, 45] have significantly reduced the computational demands of AT via *single-step attacks* and *superconvergence*.

However, today’s AT frameworks predominantly focus on a *single-attack*, i.e., they seek robustness to a single perturbation, typically ℓ_∞ -bounded [35, 40, 42, 46, 48, 45, 44, 29, 9, 39, 47, 10, 11, 14]. This results in low performance against other perturbations such as ℓ_2 , ℓ_1 , or the union of $(\ell_\infty, \ell_2, \ell_1)$. Indeed, as shown in Fig. 1, four state-of-the-art (SOTA) single-attack AT frameworks (*black markers*) employing only ℓ_∞ -bounded perturbations achieve low adversarial accuracy $\mathcal{A}_{\text{adv}}^{(U)}$ of $\approx 15\%$ -to- 20% against the union of $(\ell_\infty, \ell_2, \ell_1)$ perturbations. Recent extensions in AT [23, 37, 19] do seek higher $\mathcal{A}_{\text{adv}}^{(U)}$ but only at the expense of a $6\times$ -to- $10\times$ increase in the total training time (*blue markers in Fig. 1*). The large training time of these AT frameworks has inhibited their application to large-scale datasets such as ImageNet, e.g., Maini et al. [23], Tramèr & Boneh [37] show results for MNIST and CIFAR-10 only, while Laidlaw et al. [19] only additionally show 64×64 ImageNet-100 results.

The high training time for AT frameworks arises from two sources: (i) the need to employ larger networks, e.g., MSD [23] with ResNet-18 achieves higher $\mathcal{A}_{\text{adv}}^{(U)}$ than PAT [19] with ResNet-50 (see Fig. 1); and (ii) the need to incorporate multiple perturbations during each attack step and a higher

overall number of attack steps, *e.g.*, 50 in MSD [23], 20 in AVG [37]. Obviously one can always reduce the number of attack steps in MSD/AVG to proportionally reduce training time. Doing so results in training time and $\mathcal{A}_{\text{adv}}^{(U)}$ to rapidly approach the training complexity and $\mathcal{A}_{\text{adv}}^{(U)}$ of standard AT frameworks, *e.g.*, a 5-step MSD and 2-step AVG is equivalent in training time and accuracy to PGD and TRADES, respectively. Notwithstanding the expensive nature of 50-step multi-attack training, today MSD [23] achieves a SOTA $\mathcal{A}_{\text{adv}}^{(U)}$ of 47% with ResNet-18 on CIFAR-10.

This poses a question: can we approach the high robustness of multiple-attack AT such as 50-step MSD against the union of $(\ell_\infty, \ell_2, \ell_1)$ perturbations while maintaining the low training time of fast single-attack AT frameworks such as FreeAdv [35] and FastAdv [40]?

In our quest to answer this question we find that noise augmentation using adequately shaped noise within standard single-attack AT frameworks employing ℓ_∞ -bounded perturbations significantly improves robustness against the union of $(\ell_\infty, \ell_2, \ell_1)$ perturbations. The improvement appears to be a consequence of a well-established byproduct of AT frameworks – the reduction in the curvature of the decision boundary of networks trained using single-attack AT [6, 25]. We confirm this connection by quantifying the impact of single-attack AT on the geometric orientations of different perturbations.

Based on this insight, we propose **Shaped Noise Augmented Processing (SNAP)** – *a method to enhance robustness against the union of perturbation types by augmenting single-attack AT frameworks*. SNAP prepends a deep net with a shaped noise (SN) augmentation layer (see Fig. 4) whose distribution parameter Σ is learned with that of the network (θ) within any standard single-attack AT framework. SNAP improves the robustness of four SOTA ℓ_∞ -AT frameworks against the union of $(\ell_\infty, \ell_2, \ell_1)$ perturbations by 15%-to-20% on CIFAR-10 (red markers in Fig. 1) with only a modest ($\sim 10\%$) increase in training time. This expands the capabilities of widely popular single-attack ℓ_∞ AT frameworks to providing robustness to the union of $(\ell_\infty, \ell_2, \ell_1)$ perturbations without sacrificing training efficiency. We validate SNAP’s benefits via thorough comparisons with *nine SOTA adversarial training and randomized smoothing frameworks* across different operating regimes on both CIFAR-10 and ImageNet.

One tangible outcome of our work – we demonstrate *for the first time* ResNet-50 (ResNet-101) networks on ImageNet that achieve $\mathcal{A}_{\text{adv}}^{(U)} = 32\%$ (35%) against the union of $(\ell_\infty(\epsilon = 2/255), \ell_2(\epsilon = 2.0), \ell_1(\epsilon = 72.0))$ perturbations. Our code is available at <https://github.com/adpatil2/SNAP>.

2 Related Work

We categorize works on adversarial vulnerability of DNNs as follows:

Low-complexity adversarial training: The high computational needs of AT frameworks has spurred significant efforts in reducing their complexity [45, 35, 40, 48]. FreeAdv [35] updates weights while accumulating multiple attack iterations. FastAdv [40] employs *appropriate* use of single-step attacks, while Zheng et al. [48] leverage inter-epoch similarity between adversarial perturbations. However, these fast AT methods seek robustness against a single perturbation type, *e.g.*, ℓ_∞ norm-bounded perturbations. In contrast, SNAP expands the capabilities of these AT frameworks by enhancing robustness to the union of three perturbation types $(\ell_\infty, \ell_2, \ell_1)$, while preserving their efficiency.

Robustness against union of perturbation models: The focus on the robustness against the union of multiple perturbation types is relatively new. Kang et al. [17] studied transferability between different perturbation types, while Jordan et al. [16] considered combination attacks with low perceptual distortion. Stutz et al. [36] proposed a modification in AT to *detect* images with different models of perturbations via confidence thresholding, but they don’t attempt to *classify* perturbed images correctly. For accurate classification in the presence of different perturbation models, Tramèr &

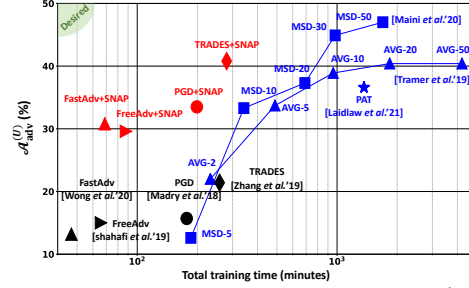


Figure 1: Adversarial accuracy ($\mathcal{A}_{\text{adv}}^{(U)}$) against union of $(\ell_\infty, \ell_2, \ell_1)$ vs. measured wall-clock total training time on CIFAR-10 with different AT frameworks on single NVIDIA TESLA P100 GPU. $\epsilon = (0.031, 0.5, 12)$ for $(\ell_\infty, \ell_2, \ell_1)$ perturbations, respectively. SNAP enhances robustness with a small increase in training time. All frameworks except PAT employ ResNet-18.

Boneh [37] studied empirical and theoretical trade-offs involved in including multiple perturbation types simultaneously during training. Maini et al. [23] further built upon this work to propose the multi steepest descent (MSD) AT framework which chooses one among the three perturbation models ($\ell_\infty, \ell_2, \ell_1$) in each attack iteration during training, achieving SOTA adversarial accuracy on CIFAR-10 against the union of the ($\ell_\infty, \ell_2, \ell_1$) perturbation models, albeit at a high ($10\times$) training time. In contrast, SNAP provides high robustness against the union of ($\ell_\infty, \ell_2, \ell_1$) perturbation models using established single-attack ℓ_∞ AT frameworks. This enables to showcase the benefits of our approach on large-scale datasets such as ImageNet.

Recently, Laidlaw et al. [19] developed a novel AT framework (PAT) with low perceptual distortion attacks to demonstrate impressive generalization to unseen attacks. In contrast, we focus on extending the capabilities of widely popular ℓ_∞ -AT frameworks to providing robustness against the union of ($\ell_\infty, \ell_2, \ell_1$) perturbations, while preserving their training efficiency.

Noise augmentation: Multiple recent works have investigated the role of randomization in enhancing adversarial robustness [12, 26, 8, 27] with theoretical guarantees. Another prominent line of work in this category is randomized smoothing [5, 33, 20, 43], where random noise is used as a tool to compute certification bounds. Rusak et al. [32] also explored the role of noise augmentation for improving the robustness against common-corruptions [13]. In contrast, in SNAP, noise augmentation is used as a means to enable widely popular ℓ_∞ -AT frameworks to efficiently achieve high robustness against the union of multiple norm-bounded perturbations. As is the characteristic of AT works, our results are primarily empirical in nature. Hence, we follow recent guidelines [38, 23] to evaluate the accuracy against the strongest possible adversaries. We do explicitly compare ℓ_∞ -AT+SNAP with randomized smoothing approaches in the Appendix B.1.

3 Subspace Analysis of Adversarial Perturbations

In this section, we employ subspace methods to comprehend the distinction between ℓ_∞, ℓ_2 and ℓ_1 perturbations. For each input $x_i \in \mathbb{R}^D$ in dataset X , consider adversarial perturbations α_i, β_i , and γ_i bounded within ℓ_∞, ℓ_2 , and ℓ_1 norms, respectively.

We begin with a hypothesis (see Fig. 2): *The perturbations α, β , and γ corresponding to input x have directions that differ significantly if the curvature of the decision boundary is high in the neighborhood of x . Conversely, if the curvature of the decision boundary is low, the perturbations α, β , and γ tend to point in similar directions.*

Since, prior works [6, 25] have found that single-attack AT reduces the curvature of the decision boundary, we test our hypothesis by studying the following two networks on CIFAR-10 data: a *non-robust* ResNet18 f_θ^{van} trained using vanilla training, and a *robust* ResNet18 f_θ^{rob} trained using the TRADES [46] AT framework employing ℓ_∞ perturbations.

We compute perturbations α_i, β_i , and γ_i for each $x_i \in X$ for both networks, i.e., $\kappa \in \{\text{van}, \text{rob}\}$. We compute the singular vector basis \mathcal{P}^κ for the set of ℓ_2 bounded perturbations $\Delta^\kappa = \{\beta_1^\kappa, \dots, \beta_{|X|}^\kappa\}$. The normalized mean squared projections of the three types of perturbation vectors on the singular vector basis \mathcal{P}^κ of vanilla trained ResNet-18 (\mathcal{P}^{van}) (Fig. 3(a)) and TRADES trained ResNet-18 (\mathcal{P}^{rob}) (Fig. 3(b)) shows a clear contrast.

The perturbations of a vanilla trained network roll-off gradually to occupy a larger subspace as indicated in Fig. 3(a). Specifically, the projections of α and γ occupy almost all 3000 directions in the basis \mathcal{P}^{van} since their mean squared projections are within $\sim 10\%$ of the maximum value m_{max} . This shows that the dominant singular vectors of β are not well-aligned with α and γ in a vanilla trained network. With TRADES AT (Fig. 3(b)), however, all three types of perturbations are *squeezed* into a much *smaller* subspace spanning only the top 250 singular vectors in the perturbation basis \mathcal{P}^{rob} . Outside these 250 dimensions, the mean squared projections fall to $< 10\%$ of their maximum value.

In summary, the results in Fig. 3 validate the hypothesis that single-attack AT increases the average alignment of different perturbation types due to the reduction in the decision boundary curvature. In

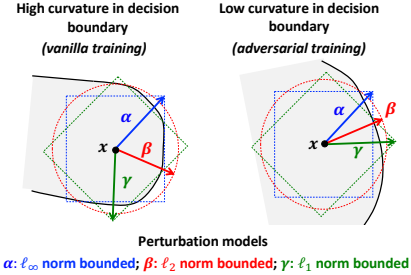


Figure 2: Illustration of the role of decision boundary curvature on the distinction between different types of perturbations α, β and γ of the given input x .

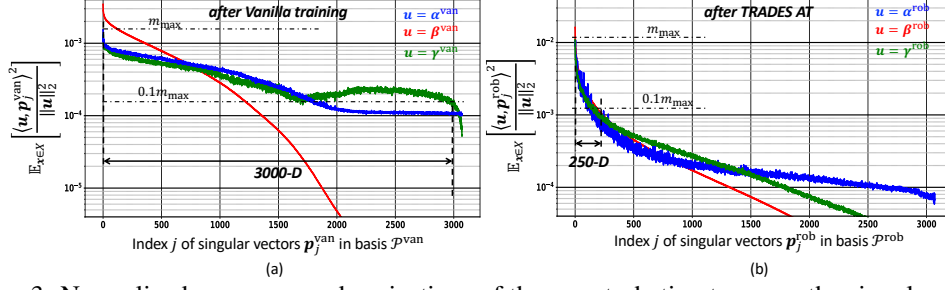


Figure 3: Normalized mean squared projections of three perturbation types on the singular vector basis \mathcal{P}^κ of ℓ_2 perturbations of ResNet18 on CIFAR-10 after: (a) vanilla training ($\kappa \equiv \text{van}$), and (b) TRADES training ($\kappa \equiv \text{rob}$). The singular vectors p_i^κ comprising $\mathcal{P}^\kappa = \{p_1^\kappa, \dots, p_D^\kappa\}$ are ordered in descending order of their singular values.

Sec. 4, we exploit this behavior of single-attack ℓ_∞ AT to improve its robustness against the union of multiple perturbation models via SNAP.

4 Shaped Noise Augmented Processing (SNAP)

We show that single-attack AT can be enhanced to address multiple perturbations by introducing noise to appropriately *wiggle* the ℓ_∞ -bounded perturbations (Fig. 4(a)). However, to do so, the noise distribution needs to be *chosen* and *shaped* appropriately to minimize its impact on natural accuracy and robustness to ℓ_∞ -bounded perturbations.

We experiment with both ℓ_∞ and ℓ_2 perturbations in single-attack AT frameworks and find ℓ_∞ -AT to be suitable for our proposed shaped noise augmentation (see Sec. 5.2.1 for details). Hence, in this section, we describe SNAP for single-attack AT frameworks employing ℓ_∞ perturbations.

4.1 SNAPnet

A deep net $f_\theta(\mathbf{x}) : \mathbb{R}^D \rightarrow \{0, 1\}^C$ parametrized by θ maps the input $\mathbf{x} \in \mathbb{R}^D$ to a one-hot vector $\mathbf{y} \in \{0, 1\}^C$ over C classes.

We construct a SNAP-based deep net (SNAPnet) $f_{\theta, \Sigma}^{\text{SN}}(\mathbf{x})$ by introducing an additive shaped noise (SN) layer (Fig. 4(b)), where the noise distribution parameter Σ is learned during training. Formally,

$$\mathbf{y} = f_{\theta, \Sigma}^{\text{SN}}(\mathbf{x}) = f_\theta(\mathbf{x} + \mathbf{n}) = f_\theta(\mathbf{x} + V\Sigma\mathbf{n}_0), \quad (1)$$

where $\mathbf{n}_0 \sim \mathcal{L}(0, \mathbf{I}_{D \times D})$ is a zero-mean isotropic Laplace noise vector, $\Sigma = \text{Diag}[\sigma_1, \dots, \sigma_D]$ is a distribution parameter denoting its per-dimension standard deviation, $\mathbf{I}_{D \times D}$ denotes the $D \times D$ identity matrix, and $V = [\mathbf{v}_1, \dots, \mathbf{v}_D]$ denotes a basis in \mathbb{R}^D . We also studied Gaussian and Uniform distributed \mathbf{n}_0 , but empirically find the Laplace distribution to yield better results (Sec. 5.2.1). We use $V = \mathbf{I}_{D \times D}$ for all our experiments in the main text and study other options for V in the Appendix.

The final classification decision d is computed via

$$d = \arg \max_c \left[\mathbb{E}_{\mathbf{n}} [\mathbf{y}] \right]_c, \quad (2)$$

where $[\mathbf{a}]_c$ denotes the c -th element of vector \mathbf{a} . Note, the shaped noise perturbs the input \mathbf{x} with a noise source $\mathbf{n} = V\Sigma\mathbf{n}_0$ (Eq. (1)). The distribution parameter Σ is learned in the presence of any standard AT method [22, 46, 35] used for learning deep net parameters θ as described next.

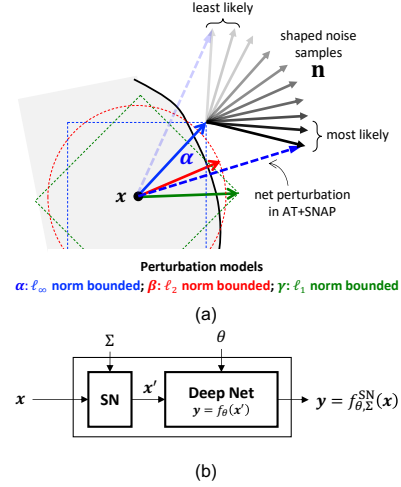


Figure 4: SNAP: (a) intuition underlying SNAP (not an exact depiction), and (b) SNAPnet $f_{\theta, \Sigma}^{\text{SN}}(\mathbf{x})$ constructed from a given deep net $f_\theta(\mathbf{x})$ by prepending a shaped noise (SN) augmentation layer which perturbs the primary input \mathbf{x} with noise \mathbf{n} whose distribution parameter Σ is learned during AT along with the base network parameter θ .

Algorithm 1 Training SNAPnet

Input: training set X ; basis $V = [v_1, \dots, v_D]$; total noise power P_{noise} ; minibatch size r ; baseline training method BASE; noise variance update frequency U_f ; Total number of epochs T

Initialize: noise variances $\Sigma_0 = \text{Diag}[\sigma_{1,0}, \dots, \sigma_{D,0}]$.

Output: robust network $f_{\theta, \Sigma}^{\text{SN}}$, noise variances $\Sigma_T = \text{Diag}[\sigma_{1,T}^2, \dots, \sigma_{D,T}^2]$.

```
1: for epoch  $t = 1 \dots T$  do
2:   for mini-batch  $B = \{x_1, \dots, x_r\}$  do    $\theta \leftarrow \text{BASE}_{\ell_\infty} \left( f_{\theta, \Sigma_t}^{\text{SN}}(\{x_i\}_{i=1}^r), \theta \right)$    ▷ BASE() Training
3:   end for
4:   if  $t \bmod U_f = 0$  then   ▷ SNAP Distribution Update once every  $U_f$  epochs
5:     for mini-batch  $B = \{x_1, \dots, x_r\}$  do
6:        $\{x_i^{\text{adv}}\}_{i=1}^r \leftarrow \text{PGD}_{\ell_2}^{(K)} \left( f_{\theta, \Sigma_t}^{\text{SN}}(\{x_i\}_{i=1}^r) \right); \quad \eta_i = x_i^{\text{adv}} - x_i \quad \forall i \in \{1, \dots, r\}$ 
7:        $\gamma_j \leftarrow \gamma_j + \sum_{i=1}^r (\langle v_j, \eta_i \rangle)^2 \quad \forall j \in \{1, \dots, D\}$    ▷ Accumulate projections; See Eq. (3)
8:     end for
9:      $\sigma_{j,t+1}^2 = P_{\text{noise}} \frac{\sqrt{\gamma_j}}{\sum_{k=1}^D \sqrt{\gamma_k}} \quad \forall j \in \{1, \dots, D\}$    ▷ Normalize accumulated projections; See Eq. (3)
10:   else
11:      $\Sigma_{t+1} \leftarrow \Sigma_t$ 
12:   end if
13: end for
```

4.2 Training SNAPnet

Algorithm 1 summarizes the procedure for training SNAPnet $f_{\theta, \Sigma}^{\text{SN}}(x)$. In each epoch, an arbitrary AT method BASE() (line 2) updates network parameters θ with input perturbed by noise \mathbf{n} . Here BASE() can be any established AT framework [22, 46, 35, 40] employing ℓ_∞ perturbation.

The SNAP parameter Σ is updated once every $U_f = 10$ epochs via a *SNAP distribution update* (lines 4-10). In this update, the per-dimension noise variance σ_j^2 is updated proportional to the root mean squared projection of the adversarial perturbations η on the basis V given a total noise constraint $\sum_{j=1}^D \sigma_j^2 = P_{\text{noise}}$, where P_{noise} denotes the total noise power. Formally,

$$\sigma_j^2 \propto \sqrt{\mathbb{E}_{x \in X} (\langle \eta, v_j \rangle^2)} \quad \text{s.t.} \quad \sum_{j=1}^D \sigma_j^2 = P_{\text{noise}}, \quad (3)$$

where η is the ℓ_2 norm-bounded PGD adversarial perturbation for the given input $x \in X$ (line 6). Note that these ℓ_2 perturbations are employed *only* for noise shaping and are distinct from the ℓ_∞ perturbations employed by BASE() AT (line 2). Also, ℓ_∞ perturbations cannot be used here since their projections are constant $\forall j$ when $V = \mathbf{I}_{D \times D}$, whereas employing ℓ_1 perturbations leads to poor shaping due to high sparsity.

Thus, in SNAP, the average squared ℓ_2 norm of the noise vector \mathbf{n} is held constant at P_{noise} while adapting the noise variances in the individual dimensions so as to align the noise vectors with the adversarial perturbations *on average*. Intuitively, the decision boundary is pushed aggressively in those directions.

4.3 Remarks

Note that the SNAP distribution update is distinct from BASE() AT. Hence, SNAP doesn't require any hyperparameter tuning in BASE(). For fairness to baselines we keep all hyperparameters identical when introducing SNAP in all our experiments. However, SNAP introduces a new hyperparameter P_{noise} , which permits to trade adversarial robustness $\mathcal{A}_{\text{adv}}^{(U)}$ for natural accuracy \mathcal{A}_{nat} . This trade-off is explored in Sec. 5.2.2.

The computational overhead of SNAP is small ($\sim 10\%$) since the *SNAP Distribution Update* occurs once in 10 epochs using just 20% of the training data to update the noise standard deviations σ_j . We provide more details about the *SNAP Distribution Update* in the Appendix.

Method	\mathcal{A}_{nat}	$\mathcal{A}_{\text{adv}}^{(\ell_\infty)}$ $\epsilon = 0.03$	$\mathcal{A}_{\text{adv}}^{(\ell_2)}$ $\epsilon = 0.5$	$\mathcal{A}_{\text{adv}}^{(\ell_1)}$ $\epsilon = 12$	$\mathcal{A}_{\text{adv}}^{(U)}$
PGD AT with ℓ_∞ perturbations					
PGD	84.6	48.8	62.3	15.0	15.0
+SNAP[G]	80.7	45.7	66.9	34.6	31.9
+SNAP[U]	85.1	42.7	66.7	28.6	26.6
+SNAP[L]	83.0	44.8	68.6	40.1	35.6
PGD AT with ℓ_2 perturbations					
PGD	89.3	28.8	67.3	31.8	25.1
+SNAP[G]	83.0	35.0	65.8	39.9	30.2
+SNAP[U]	86.4	32.3	66.7	30.2	25.0
+SNAP[L]	84.8	33.4	66.1	42.5	30.8

Table 1: ResNet-18 CIFAR-10 results showing the impact of SNAP augmentation of PGD [22] AT framework with ℓ_∞ (top) and ℓ_2 (bottom) perturbations where [G], [U], and [L], denote shaped Gaussian, Uniform, and Laplace noise.

Method	\mathcal{A}_{nat}	$\mathcal{A}_{\text{adv}}^{(\ell_\infty)}$ $\epsilon = 0.03$	$\mathcal{A}_{\text{adv}}^{(\ell_2)}$ $\epsilon = 0.5$	$\mathcal{A}_{\text{adv}}^{(\ell_1)}$ $\epsilon = 12$	$\mathcal{A}_{\text{adv}}^{(U)}$
High Complexity AT with ℓ_∞ perturbations					
PGD	84.6	48.8	62.3	15.0	15.0
+SNAP	83.0	44.8	68.6	40.1	35.6
TRADES	82.1	50.2	59.6	19.8	19.7
+SNAP	80.9	45.2	66.9	46.6	41.2
Low Complexity AT with ℓ_∞ perturbations					
FreeAdv	81.7	46.1	59	15.0	15.0
+SNAP	83.5	39.7	66.2	34.3	29.6
FastAdv	85.7	46.2	60.0	13.2	13.2
+SNAP	84.2	40.4	67.9	36.6	30.8

Table 2: ResNet-18 CIFAR-10 results showing the impact of SNAP augmentation of established ℓ_∞ -AT frameworks. The computational overhead of SNAP is limited to $\sim 10\%$.

5 Experimental Results

5.1 Setup

Following experimental settings of prior work [46, 35, 23], we employ a ResNet-18 network for CIFAR-10 experiments and both ResNet-50 and ResNet-101 networks for ImageNet experiments. Accuracy on clean test data is referred to with \mathcal{A}_{nat} and accuracy on adversarially perturbed test data is referred to via $\mathcal{A}_{\text{adv}}^{(\ell_\infty)}$, $\mathcal{A}_{\text{adv}}^{(\ell_2)}$, and $\mathcal{A}_{\text{adv}}^{(\ell_1)}$, for ℓ_∞ , ℓ_2 , and ℓ_1 norm bounded perturbations, respectively. Accuracy against the *union* of all three perturbations is denoted by $\mathcal{A}_{\text{adv}}^{(U)}$.

For a fair robustness comparison, our evaluation setup closely follows the setup of Maini et al. [23] for CIFAR-10 data: (1) choose norm bounds $\epsilon = (0.031, 0.5, 12.0)$ for $(\ell_\infty, \ell_2, \ell_1)$ perturbations, respectively; (2) scale norm bounds for images to lie between $[0, 1]$; (3) choose the PGD attack configuration to be *100 iterations with 10 random restarts* for all perturbation types¹; and (4) estimate $\mathcal{A}_{\text{adv}}^{(U)}$ as the fraction of test data that is *simultaneously* resistant to all three perturbation models.

Following the guidelines of Tramer et al. [38], we carefully design *adaptive* PGD attacks that target the full defense – SN layer – since SNAPnet is end-to-end differentiable. Specifically, we backpropagate to primary input \mathbf{x} through the SN layer (see Fig. 4). Thus, the final shaped noise distribution is exposed to the adversary. We also account for the expectation $\mathbb{E}_{\mathbf{n}}[\cdot]$ in Eq. (2) by explicitly averaging deep net logits over $N_0 (= 8)$ noise samples *before* computing the gradient, which eliminates any gradient obfuscation, and is known to be the strongest attack against noise augmented models [33]. In the Appendix A we also show robustness stress tests and evaluate more attacks.

On CIFAR-10 data, we compare with the following seven key SOTA AT frameworks: PGD [22], TRADES [46], FreeAdv [35], FastAdv [40], AVG [37], MSD [23], PAT [19]. We also compare with two randomized smoothing frameworks [5, 33] in the Appendix B.1. Thanks to their GitHub code releases, we first successfully reproduce their results with a ResNet-18 network in our environment. In the case of PAT [19], we evaluate and compare with their pretrained ResNet-50 model on CIFAR-10. We compare all training times on a single NVIDIA P100 GPU. On ImageNet data, we primarily compare to FreeAdv [35]. We train ResNet-50 and its SNAPnet version with FreeAdv on a Google Cloud server with four NVIDIA P100 GPUs to compare their accuracy and training times. We provide all hyperparameters in Appendix C. Our code and pretrained models are available at <https://github.com/adpatil2/SNAP>.

5.2 Ablation Studies

5.2.1 Impact of Noise Distribution and Model of BASE() AT Perturbations

In this subsection, we first study the impact of employing ℓ_∞ vs. ℓ_2 perturbations in BASE AT() (see line 2 in Alg. 1) on $\mathcal{A}_{\text{adv}}^{(U)}$. For each choice, we further experiment with three distributions for the

¹Following Maini et al. [23], we also run all attacks on a subset of the first 1000 test examples with 10 random restarts for CIFAR-10 data.

SN layer in Fig. 4(b) viz. Gaussian, Uniform, and Laplace. We don’t consider ℓ_1 perturbations in BASE AT() since Maini et al. [23] showed that employing ℓ_1 single-attack AT achieves very low robustness to all attacks. We choose PGD [22] AT as BASE AT() for this ablation study. For a fair comparison across the noise distributions, we fix $P_{\text{noise}} = 160$, enforcing all noise vectors to have the same average ℓ_2 norm. For each distribution, the noise is shaped per the procedure summarized in Alg. 1.

As observed in Table 1, ℓ_∞ -PGD AT achieves much lower $\mathcal{A}_{\text{adv}}^{(U)}$ than ℓ_2 -PGD AT, an observation also reported by Maini et al. [23]. With SNAP, however, we find that there is an interaction between the perturbation model in PGD AT and the noise distribution in SNAP. For instance, SNAP[U] enhances $\mathcal{A}_{\text{adv}}^{(U)}$ by 11% with ℓ_∞ -PGD AT while not achieving any improvement with ℓ_2 -PGD AT. In fact, SNAP appears to be particularly suitable for ℓ_∞ -AT, since it always improves $\mathcal{A}_{\text{adv}}^{(U)}$ by 11%-to-20.6% irrespective of the noise distribution.

Finally, of the three noise distributions, we find the Laplace distribution to be distinctly superior, achieving the highest $\mathcal{A}_{\text{adv}}^{(U)}$ (35.6% and 30.8%) due to a significant improvement in $\mathcal{A}_{\text{adv}}^{(\ell_1)}$ for both ℓ_∞ and ℓ_2 PGD AT, respectively. The superiority of the Laplace distribution in achieving high $\mathcal{A}_{\text{adv}}^{(\ell_1)}$ stems from its heavier tail compared to the Gaussian and Uniform distributions with the same variance. Shaped Laplace noise generates the highest fraction of extreme values in a given noise sample. Hence, it is more effective in improving accuracy against ℓ_1 -bounded attacks, which are the strongest when perturbing few pixels by a large magnitude [23, 37]. We discuss this further in the Appendix B.7. Henceforth, unless otherwise mentioned, we choose Laplace noise for SNAP and ℓ_∞ perturbations for BASE() AT as the default setting since it achieves the highest $\mathcal{A}_{\text{adv}}^{(U)}$.

5.2.2 Impact of P_{noise}

Next, we explore the impact of the SNAP hyperparameter P_{noise} , which constrains the average squared ℓ_2 norm of the noise vector \mathbf{n} . It enables to trade between adversarial and natural accuracy.

Fig. 5 shows that, as P_{noise} increases, $\mathcal{A}_{\text{adv}}^{(\ell_1)}$ improves from 31% to 47%, accompanied by a graceful (5%) drop in \mathcal{A}_{nat} and a small drop of 2% in $\mathcal{A}_{\text{adv}}^{(\ell_\infty)}$ that stabilizes to $\approx 45\%$. These results show: (1) SNAP preserves the impact of ℓ_∞ perturbations which is not surprising since PGD AT [22] explicitly includes those, and (2) P_{noise} provides an explicit knob to control the \mathcal{A}_{nat} vs. \mathcal{A}_{adv} trade-off. Henceforth, we choose P_{noise} values that incur $< 1.5\%$ drop in \mathcal{A}_{nat} for all SNAP+AT experiments.

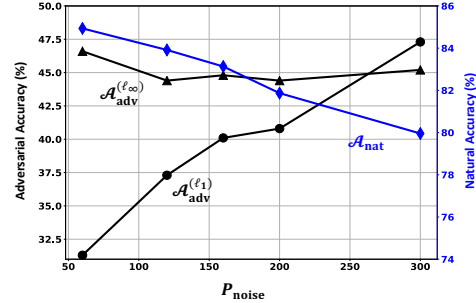


Figure 5: ResNet-18 CIFAR-10 results: adversarial accuracy $\mathcal{A}_{\text{adv}}^{(\ell_1)}$, $\mathcal{A}_{\text{adv}}^{(\ell_\infty)}$, and natural accuracy \mathcal{A}_{nat} vs. total noise power P_{noise} for PGD+SNAP.

5.2.3 SNAP augmented SOTA AT Frameworks

Table 2 shows the effectiveness of SNAP for four SOTA AT frameworks: high complexity frameworks, such as PGD [22], TRADES [46], and low complexity frameworks such as FreeAdv [35], FastAdv [40]. All are trained against ℓ_∞ attacks with $\epsilon = 0.031$. As expected, while they achieve high $\mathcal{A}_{\text{adv}}^{(\ell_\infty)}$, their $\mathcal{A}_{\text{adv}}^{(\ell_2)}$ and $\mathcal{A}_{\text{adv}}^{(\ell_1)}$ are lower.

For high-complexity AT, SNAP enhances $\mathcal{A}_{\text{adv}}^{(\ell_2)}$ and $\mathcal{A}_{\text{adv}}^{(\ell_1)}$ by $\sim 6\%$ and $\sim 25\%$, respectively, while incurring only a drop of $\sim 5\%$ in $\mathcal{A}_{\text{adv}}^{(\ell_\infty)}$. Thus overall, SNAP improves robustness ($\mathcal{A}_{\text{adv}}^{(U)}$) by $\sim 20\%$ against the union of the three perturbation models. Note that this robustness improvement comes at only a $\sim 1\%$ drop in \mathcal{A}_{nat} (see Table 2). For low-complexity ATs, SNAP improvements in union robustness ($\mathcal{A}_{\text{adv}}^{(U)}$) are also significant ($\sim 15\%$). Again, presence of SNAP improves $\mathcal{A}_{\text{adv}}^{(\ell_2)}$ and $\mathcal{A}_{\text{adv}}^{(\ell_1)}$. This time the drop in $\mathcal{A}_{\text{adv}}^{(\ell_\infty)}$ is $\sim 7\%$. We believe this is due to the fact that these frameworks employ weaker single-step attacks during training. Note that in the case of FreeAdv+SNAP, we actually observe a $\sim 2\%$ increase in \mathcal{A}_{nat} , a trend we also observe in the ImageNet experiments described later.

Method	LR schedule	Epochs	\mathcal{A}_{nat}	$\mathcal{A}_{\text{adv}}^{(U)}$	Total time (minutes)
Set A: Total Time ≥ 12 Hrs					
AVG 50 Step [37]	cyclic	50	84.8	40.4	4217
AVG 20 Step [37]	cyclic	50	85.6	40.4	1834
AVG 10 Step [37]	cyclic	50	86.7	38.9	956
PAT [19]	step	100	82.4	36.6	1364
MSD 50 Step [23]	cyclic	50	81.7	47.0	1693
MSD 30 Step [23]	cyclic	50	82.4	44.9	978
Set B: 8 Hrs < Total Time < 12 Hrs					
AVG 5 Step [37]	cyclic	50	87.8	33.7	489
MSD 20 Step [23]	cyclic	50	83.0	37.3	690
TRADES [46]	step	100	82.0	19.7	516
TRADES+SNAP	step	100	80.9	41.2	566
Set C: 5 Hrs < Total Time < 8 Hrs					
MSD 10 Step [23]	cyclic	50	83.6	33.3	342
PGD [22]	step	100	84.6	15.0	354
PGD+SNAP	step	100	83.0	35.6	403
Set D: 2 Hrs < Total Time < 5 Hrs					
AVG 2 Step [37]	cyclic	50	88.4	22.0	232
MSD 5 Step [23]	cyclic	50	84.0	12.6	185
PGD [22]	cyclic	50	82.8	15.7	177
TRADES [46]	cyclic	50	80.0	21.4	258
PGD+SNAP	cyclic	50	82.3	33.5	199
TRADES+SNAP	cyclic	50	78.8	40.8	280
Set E: Total Time < 2 Hrs					
FreeAdv [35]	step	200	81.7	15.0	66
FastAdv [40]	cyclic	50	85.7	13.2	47
FreeAdv+SNAP	step	200	83.5	29.6	88
FastAdv+SNAP	cyclic	50	84.2	30.8	69

Table 3: CIFAR-10 results for comparing adversarial accuracy $\mathcal{A}_{\text{adv}}^{(U)}$ vs. training time (on single NVIDIA P100 GPU) for different AT frameworks and the improvements by introducing proposed SNAP technique. All frameworks except PAT [19] (which employs ResNet-50) employ ResNet-18.

Training	\mathcal{A}_{nat} (%)	$\mathcal{A}_{\text{adv}}^{(\ell_{\infty})}$ $\epsilon = 2/255$	$\mathcal{A}_{\text{adv}}^{(\ell_2)}$ $\epsilon = 2.0$	$\mathcal{A}_{\text{adv}}^{(\ell_1)}$ $\epsilon = 72.0$	$\mathcal{A}_{\text{adv}}^{(U)}$	Total time (minutes)
ResNet-50						
FreeAdv [35]	61.7	47.8	19.9	14.8	12.6	3590
FreeAdv+SNAP	66.8	46.1	37.8	37.4	32.4	3756
ResNet-101						
FreeAdv [35]	65.4	51.8	22.8	18.8	16.1	5678
FreeAdv+SNAP	69.7	50.3	41.1	40.2	35.4	5904

Table 4: ImageNet results: Iso-hyperparameter introduction of SNAP yields $\sim 20\%$ improvement in adversarial accuracy ($\mathcal{A}_{\text{adv}}^{(U)}$) with modest impact on training time for ResNet-50 and ResNet-101.

5.3 Robustness vs. Training Complexity

Next we quantify adversarial robustness vs. training time trade-offs. Table 3 shows that SNAP augmentation of single-attack AT frameworks achieves the highest $\mathcal{A}_{\text{adv}}^{(U)}$, when training time is constrained to 12 hours (sets **B**, **C**, **D**, and **E**).

For instance, TRADES+SNAP achieves a 4% higher $\mathcal{A}_{\text{adv}}^{(U)}$ ($= 41\%$) than MSD-20 with 2 hours *lower* training time (Set **B** in Table 3). Similarly, PGD+SNAP achieves a 2% higher $\mathcal{A}_{\text{adv}}^{(U)}$ than MSD-10 while having a similar training time (Set **C**). Note that both PGD and TRADES here use 100 training epochs with standard step learning rate (LR) schedule, while MSD frameworks employ a cyclic learning rate schedule to achieve superconvergence in 50 epochs.

In Set **D**, following Maini et al. [23], we employ a cyclic learning rate schedule for PGD, TRADES, as well as for PGD+SNAP and TRADES+SNAP to achieve convergence in 50 epochs. Improvements in $\mathcal{A}_{\text{adv}}^{(U)}$ for PGD+SNAP and TRADES+SNAP are similar to those in Sets **B** and **C**. Most notably,

PGD+SNAP with cyclic learning rate achieves $\sim 20\%$ and 11.5% *higher* $\mathcal{A}_{\text{adv}}^{(U)}$ than MSD-5 and AVG-2, respectively, while having a similar training time (~ 3 hours). Set **E** augments the data from Table 2 with training times. FastAdv+SNAP and FreeAdv+SNAP achieve a high $\mathcal{A}_{\text{adv}}^{(U)} \sim 30\%$, while preserving the training efficiency of both FastAdv and FreeAdv. Notably, FastAdv+SNAP achieves 18% higher $\mathcal{A}_{\text{adv}}^{(U)}$ than MSD-5, while being $\sim 2.7\times$ more efficient to train.

5.4 ImageNet Results

Thanks to SNAP’s low computational overhead combined with FreeAdv’s fast training time, we are for the first time able to report adversarial accuracy of ResNet-50 and ResNet-101 against the union of $(\ell_\infty, \ell_2, \ell_1)$ attacks on ImageNet.

We closely follow the evaluation setup of Shafahi et al. [35]. Specifically, we use 100 step PGD attack, one of the strongest adversaries considered by Shafahi et al. [35], and evaluate on the entire test set. We first reproduce FreeAdv [35] results using the *same* hyperparameters and then introduce SNAP. All hyperparameter details are specified in the Appendix.

In order to clearly demonstrate the contrast between robustness to different perturbation models, we evaluate with $\epsilon = (2/255, 2.0, 72.0)$ for $(\ell_\infty, \ell_2, \ell_1)$ attacks, respectively.² As shown in Table 4, FreeAdv achieves a high $\mathcal{A}_{\text{adv}}^{(\ell_\infty)} = 47.8\%$ with ResNet-50, but a lower $\mathcal{A}_{\text{adv}}^{(\ell_2)} = 20\%$ and $\mathcal{A}_{\text{adv}}^{(\ell_1)} = 15\%$, and consequently, a low $\mathcal{A}_{\text{adv}}^{(U)}$ of 12.6% against the union of the perturbations. In contrast, FreeAdv+SNAP improves $\mathcal{A}_{\text{adv}}^{(\ell_2)}$ and $\mathcal{A}_{\text{adv}}^{(\ell_1)}$ by 17% and 22% , respectively, accompanied by a 5% improvement in \mathcal{A}_{nat} and a small 2% loss in $\mathcal{A}_{\text{adv}}^{(\ell_\infty)}$. This results in an overall robustness improvement of 20% against the union of the perturbation models, setting a first benchmark for ResNet-50 on ImageNet. Upon increasing the network to ResNet-101, both natural and adversarial accuracies improve by $\approx 4\%$ for FreeAdv, a trend also observed by Shafahi et al. [35]. SNAP further improves FreeAdv’s results for \mathcal{A}_{nat} and $\mathcal{A}_{\text{adv}}^{(U)}$ by 4.3% and 19.3% .

6 Discussion

Given the wide popularity of ℓ_∞ -AT, in this paper, we propose SNAP as an augmentation that generalizes the effectiveness of ℓ_∞ -AT to the union of $(\ell_\infty, \ell_2, \ell_1)$ perturbations. SNAP’s strength is its simplicity and efficiency. Consequently, this work sets a first benchmark for ResNet-50 and ResNet-101 networks which are resilient to the union of $(\ell_\infty, \ell_2, \ell_1)$ perturbations on ImageNet. Note that norm-bounded perturbations include a large class of attacks, *e.g.*, gradient-based [22, 31, 37, 23, 4, 24], decision-based [3] and black-box [1] attacks.

More work is needed to extend the proposed SNAP technique to attacks beyond norm-bounded additive perturbations, *e.g.*, functional [18, 41], rotation [7], texture [2], etc. We provide preliminary evaluations in this direction in the Appendix. It is important to note that SNAP is meant to be an efficient technique for improving ℓ_∞ -AT, and *not* a new defense. Indeed defending against a large variety of attacks simultaneously remains an open problem, with encouraging results from recent efforts [23, 19].

Another limitation of our approach is that its benefits are demonstrated empirically. It is an inevitable consequence of a lack of any theoretical guarantees for underlying AT frameworks. An interesting direction of future work is to explore whether any theoretical guarantees can be derived for anisotropic shaped noise distributions in SNAP by building upon the recent developments in randomized smoothing [33, 43]. This could be a potential avenue for bridging the gap between certification bounds and empirical adversarial accuracy.

Finally, we believe that any effort on improving adversarial robustness of deep nets has net positive societal impact. However, recent past in this field has shown that any improvements in defense techniques also lead to more effective threat models. While such a cat-and-mouse game is of great intellectual value in the academic setting, it does have an unintentional negative societal consequence of equipping malicious outside actors with a broad set of tools. This further underscores the well-recognized need for provable defenses.

²Note that ℓ_2 and ℓ_1 norms of PGD perturbation with ℓ_∞ norm of $2/255$ can be as large as ~ 3.0 and ~ 1100 for images of size $224 \times 224 \times 3$.

References

- [1] Andriushchenko, M., Croce, F., Flammarion, N., and Hein, M. Square attack: a query-efficient black-box adversarial attack via random search. In *European Conference on Computer Vision*, pp. 484–501. Springer, 2020.
- [2] Bhattad, A., Chong, M. J., Liang, K., Li, B., and Forsyth, D. A. Unrestricted adversarial examples via semantic manipulation. *arXiv preprint arXiv:1904.06347*, 2019.
- [3] Brendel, W., Rauber, J., and Bethge, M. Decision-based adversarial attacks: Reliable attacks against black-box machine learning models. In *International Conference on Learning Representations*, 2018.
- [4] Chen, P.-Y., Sharma, Y., Zhang, H., Yi, J., and Hsieh, C.-J. Ead: elastic-net attacks to deep neural networks via adversarial examples. In *Thirty-second AAAI conference on artificial intelligence*, 2018.
- [5] Cohen, J., Rosenfeld, E., and Kolter, Z. Certified adversarial robustness via randomized smoothing. In *International Conference on Machine Learning (ICML)*, 2019.
- [6] Dezfooli, S. M. M., Fawzi, A., Fawzi, O., Frossard, P., and Soatto, S. Robustness of classifiers to universal perturbations: A geometric perspective. In *International Conference on Learning Representations (ICLR)*, 2018.
- [7] Engstrom, L., Tran, B., Tsipras, D., Schmidt, L., and Madry, A. Exploring the landscape of spatial robustness. In *International Conference on Machine Learning*, pp. 1802–1811. PMLR, 2019.
- [8] Gilmer, J., Ford, N., Carlini, N., and Cubuk, E. Adversarial examples are a natural consequence of test error in noise. In *International Conference on Machine Learning*, pp. 2280–2289, 2019.
- [9] Gowal, S., Qin, C., Uesato, J., Mann, T., and Kohli, P. Uncovering the limits of adversarial training against norm-bounded adversarial examples. *arXiv preprint arXiv:2010.03593*, 2020.
- [10] Gui, S., Wang, H., Yu, C., Yang, H., Wang, Z., and Liu, J. Model compression with adversarial robustness: A unified optimization framework. *arXiv preprint arXiv:1902.03538*, 2019.
- [11] Guo, M., Yang, Y., Xu, R., Liu, Z., and Lin, D. When nas meets robustness: In search of robust architectures against adversarial attacks. In *Proceedings of the IEEE/CVF Conference on Computer Vision and Pattern Recognition*, pp. 631–640, 2020.
- [12] He, Z., Rakin, A. S., and Fan, D. Parametric noise injection: Trainable randomness to improve deep neural network robustness against adversarial attack. In *Proceedings of the IEEE Conference on Computer Vision and Pattern Recognition (CVPR)*, 2019.
- [13] Hendrycks, D. and Dietterich, T. Benchmarking neural network robustness to common corruptions and perturbations. In *International Conference on Learning Representations*, 2018.
- [14] Hu, T.-K., Chen, T., Wang, H., and Wang, Z. Triple wins: Boosting accuracy, robustness and efficiency together by enabling input-adaptive inference. *arXiv preprint arXiv:2002.10025*, 2020.
- [15] Ilyas, A., Santurkar, S., Tsipras, D., Engstrom, L., Tran, B., and Madry, A. Adversarial examples are not bugs, they are features. *arXiv preprint arXiv:1905.02175*, 2019.
- [16] Jordan, M., Manoj, N., Goel, S., and Dimakis, A. G. Quantifying perceptual distortion of adversarial examples. *arXiv preprint arXiv:1902.08265*, 2019.
- [17] Kang, D., Sun, Y., Brown, T., Hendrycks, D., and Steinhardt, J. Transfer of adversarial robustness between perturbation types. *arXiv preprint arXiv:1905.01034*, 2019.
- [18] Laidlaw, C. and Feizi, S. Functional adversarial attacks. *Advances in Neural Information Processing Systems*, 2019.
- [19] Laidlaw, C., Singla, S., and Feizi, S. Perceptual adversarial robustness: Defense against unseen threat models. *International Conference on Learning Representations (ICLR)*, 2018.
- [20] Li, B., Chen, C., Wang, W., and Duke, L. C. Certified adversarial robustness with addition gaussian noise. *Neural Information Processing Systems (NeurIPS)*, 2019.
- [21] Madaan, D., Shin, J., and Hwang, S. J. Learning to generate noise for robustness against multiple perturbations. *arXiv preprint arXiv:2006.12135*, 2020.

- [22] Madry, A., Makelov, A., Schmidt, L., Tsipras, D., and Vladu, A. Towards deep learning models resistant to adversarial attacks. *International Conference on Learning Representations (ICLR)*, 2018.
- [23] Maini, P., Wong, E., and Kolter, J. Z. Adversarial robustness against the union of multiple perturbation models. In *International Conference on Machine Learning (ICML)*, 2020.
- [24] Moosavi-Dezfooli, S.-M., Fawzi, A., and Frossard, P. Deepfool: a simple and accurate method to fool deep neural networks. In *Proceedings of the IEEE conference on computer vision and pattern recognition (CVPR)*, 2016.
- [25] Moosavi-Dezfooli, S.-M., Fawzi, A., Uesato, J., and Frossard, P. Robustness via curvature regularization, and vice versa. In *Proceedings of the IEEE Conference on Computer Vision and Pattern Recognition (CVPR)*, 2019.
- [26] Pinot, R., Meunier, L., Araujo, A., Kashima, H., Yger, F., Gouy-Pailler, C., and Atif, J. Theoretical evidence for adversarial robustness through randomization: the case of the exponential family. In *Advances in Neural Information Processing Systems*, 2019.
- [27] Pinot, R., Ettegui, R., Rizk, G., Chevalere, Y., and Atif, J. Randomization matters. how to defend against strong adversarial attacks. In *International Conference on Machine Learning (ICML)*, 2020.
- [28] Rauber, J., Zimmermann, R., Bethge, M., and Brendel, W. Foolbox native: Fast adversarial attacks to benchmark the robustness of machine learning models in pytorch, tensorflow, and jax. *Journal of Open Source Software*, 5(53):2607, 2020. doi: 10.21105/joss.02607. URL <https://doi.org/10.21105/joss.02607>.
- [29] Rebuffi, S.-A., Goyal, S., Calian, D. A., Stumberg, F., Wiles, O., and Mann, T. Fixing data augmentation to improve adversarial robustness. *arXiv preprint arXiv:2103.01946*, 2021.
- [30] Rice, L., Wong, E., and Kolter, Z. Overfitting in adversarially robust deep learning. In *International Conference on Machine Learning*, pp. 8093–8104. PMLR, 2020.
- [31] Rony, J., Hafemann, L. G., Oliveira, L. S., Ayed, I. B., Sabourin, R., and Granger, E. Decoupling direction and norm for efficient gradient-based l2 adversarial attacks and defenses. In *Proceedings of the IEEE/CVF Conference on Computer Vision and Pattern Recognition*, pp. 4322–4330, 2019.
- [32] Rusak, E., Schott, L., Zimmermann, R. S., Bitterwolf, J., Bringmann, O., Bethge, M., and Brendel, W. A simple way to make neural networks robust against diverse image corruptions. In *European Conference on Computer Vision*, pp. 53–69. Springer, 2020.
- [33] Salman, H., Li, J., Razenshteyn, I., Zhang, P., Zhang, H., Bubeck, S., and Yang, G. Provably robust deep learning via adversarially trained smoothed classifiers. In *Advances in Neural Information Processing Systems*, pp. 11289–11300, 2019.
- [34] Santurkar, S., Ilyas, A., Tsipras, D., Engstrom, L., Tran, B., and Madry, A. Image synthesis with a single (robust) classifier. In *Advances in Neural Information Processing Systems*, pp. 1262–1273, 2019.
- [35] Shafahi, A., Najibi, M., Ghiasi, A., Xu, Z., Dickerson, J., Studer, C., Davis, L. S., Taylor, G., and Goldstein, T. Adversarial training for free! *Advances in Neural Information Processing Systems (NeurIPS)*, 2019.
- [36] Stutz, D., Hein, M., and Schiele, B. Confidence-calibrated adversarial training: Generalizing to unseen attacks. In *International Conference on Machine Learning*, pp. 9155–9166. PMLR, 2020.
- [37] Tramèr, F. and Boneh, D. Adversarial training and robustness for multiple perturbations. In *Advances in Neural Information Processing Systems*, pp. 5858–5868, 2019.
- [38] Tramer, F., Carlini, N., Brendel, W., and Madry, A. On adaptive attacks to adversarial example defenses. *arXiv preprint arXiv:2002.08347*, 2020.
- [39] Vivek, B. and Babu, R. V. Single-step adversarial training with dropout scheduling. In *2020 IEEE/CVF Conference on Computer Vision and Pattern Recognition (CVPR)*, pp. 947–956. IEEE, 2020.
- [40] Wong, E., Rice, L., and Kolter, J. Z. Fast is better than free: Revisiting adversarial training. In *International Conference on Machine Learning (ICLR)*, 2020.
- [41] Xiao, C., Zhu, J.-Y., Li, B., He, W., Liu, M., and Song, D. Spatially transformed adversarial examples. In *International Conference on Learning Representations*, 2018.
- [42] Xie, C. and Yuille, A. Intriguing properties of adversarial training at scale. In *International Conference on Learning Representations*, 2020.

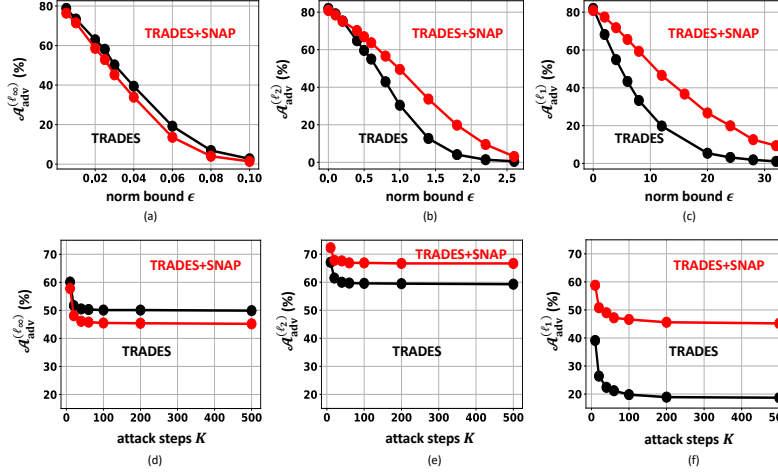


Figure 6: ResNet-18 CIFAR-10 results: Adversarial accuracy vs. norm bound ϵ for: (a) ℓ_∞ , (b) ℓ_2 , (c) ℓ_1 PGD-100 attack. Adversarial accuracy vs. attack steps K for (d) ℓ_∞ ($\epsilon = 0.031$), (e) ℓ_2 ($\epsilon = 0.5$), (f) ℓ_1 ($\epsilon = 12$) PGD-100 attacks.

- [43] Yang, G., Duan, T., Hu, E., Salman, H., Razenshteyn, I., and Li, J. Randomized smoothing of all shapes and sizes. *International Conference on Machine Learning (ICML)*, 2020.
- [44] Yang, Y.-Y., Rashtchian, C., Zhang, H., Salakhutdinov, R., and Chaudhuri, K. A closer look at accuracy vs. robustness. *Advances in Neural Information Processing Systems*, 33, 2020.
- [45] Zhang, D., Zhang, T., Lu, Y., Zhu, Z., and Dong, B. You only propagate once: Accelerating adversarial training via maximal principle. *arXiv preprint arXiv:1905.00877*, 2019.
- [46] Zhang, H., Yu, Y., Jiao, J., Xing, E., El Ghaoui, L., and Jordan, M. Theoretically principled trade-off between robustness and accuracy. In *International Conference on Machine Learning (ICML)*, 2019.
- [47] Zhang, J., Xu, X., Han, B., Niu, G., Cui, L., Sugiyama, M., and Kankanhalli, M. Attacks which do not kill training make adversarial learning stronger. In *International Conference on Machine Learning*, pp. 11278–11287. PMLR, 2020.
- [48] Zheng, H., Zhang, Z., Gu, J., Lee, H., and Prakash, A. Efficient adversarial training with transferable adversarial examples. In *Proceedings of the IEEE/CVF Conference on Computer Vision and Pattern Recognition*, pp. 1181–1190, 2020.

Appendix A Robustness Stress Tests

We conduct robustness stress tests to confirm that the benefits of SNAP are sustained for a range of attack norm-bounds, larger number of attack steps, and even for “gradient-free” attacks. For these experiments, we consider networks trained using TRADES and TRADES+SNAP (rows in Table 2 of the main paper), since they achieve the highest $\mathcal{A}_{\text{adv}}^{(U)}$ among the four SOTA AT frameworks.

A.1 Sweeping norm-bounds and number of attack steps

We sweep the number of PGD attack steps (K) and norm-bounds (ϵ) for all three perturbations ($\ell_\infty, \ell_2, \ell_1$) to confirm that the robustness gains from SNAP are achieved for a wider range of attack norm bounds, and are sustained even after increasing attack steps.

Fig. 6(a)-(c) validates the main text Table 2 conclusion that TRADES+SNAP achieves large gains ($\sim 20\%$) in $\mathcal{A}_{\text{adv}}^{(\ell_1)}$ and $\mathcal{A}_{\text{adv}}^{(\ell_2)}$ with a small ($\sim 4\%$) drop in $\mathcal{A}_{\text{adv}}^{(\ell_\infty)}$. Furthermore, this conclusion holds for a large range of ϵ values for all three perturbations. Additionally, the gain in $\mathcal{A}_{\text{adv}}^{(\ell_2)}$ due to SNAP at $\epsilon = 1.2$ is greater than the one reported in Table 2 for $\epsilon = 0.5$.

Now we increase the attack steps K to 500 and observe the impact on adversarial accuracy against ($\ell_\infty, \ell_2, \ell_1$) perturbations in Fig. 6(d,e,f), respectively. In all cases, we observe hardly any change

	TRADES	TRADES+SNAP
Natural Accuracy	82.1	80.9
DDN [31] ($\epsilon = 0.5$)	59.7	65.8
Boundary [3] ($\epsilon = 0.5$)	63.5	67.0
Square [1] ($\epsilon = 0.5$)	68.2	72.7

Table 5: ResNet-18 CIFAR-10 results showing natural accuracy (%) and adversarial accuracy (%) against ℓ_2 norm bounded DDN attack [31], boundary attack [3], and Square [1] for TRADES and TRADES+SNAP networks from Table 2 in the main text.

of the adversarial accuracy beyond $K = 100$. Hence, as noted in the main text, we have chosen $K = 100$ for all our experiments in the main text and in this supplementary.

Recall we employ 10 random restarts as recommended by Maini et al. [23] for *all* our adversarial accuracy evaluations on CIFAR-10 data.

A.2 Evaluating robustness against new attacks

We evaluate adversarial accuracy against the recent DDN [31], Boundary [3], and Square [1] attacks. The DDN attack was shown to be one of the SOTA gradient-based attacks, while boundary attack is one of the strongest “gradient-free” attacks. Of all the attacks considered in Maini et al. [23], PGD turns out to be the strongest for ℓ_∞ and ℓ_1 perturbations. Hence, in this section, we evaluate against ℓ_2 norm-bounded DDN, boundary, and Square attacks.

Following Maini et al. [23], we use the FoolBox [28] implementation of the boundary attack, which uses 25 trials per iteration. For the DDN attack, we use 100 attack steps with appropriate logit averaging for $N_0 = 8$ noise samples *before* computing the gradient in each step (similar to our PGD attack implementations). As mentioned in the main text, it eliminates any gradient obfuscation due to the presence of noise.

Table 5 shows that SNAP improves adversarial accuracy against the DDN attack by $\sim 6\%$. This is similar to improvements seen against ℓ_2 -PGD attack in Table 2 in the main text. Similarly, TRADES+SNAP achieves 3.5% (4.5%) higher adversarial accuracy than TRADES against the Boundary [3] (Square [1]) attack.

Appendix B Additional Results

B.1 Comparison with Randomized Smoothing (RS)

In this subsection, we compare with two SOTA randomized smoothing (RS) works, namely, RandSmooth [5], and SmoothAdv [33]. They employ isotropic Gaussian noise. In Fig. 7(a), we find that PGD+SNAP achieves a better \mathcal{A}_{nat} vs. $\mathcal{A}_{\text{adv}}^{(U)}$ trade-off compared to both RandSmooth [5], and SmoothAdv [33]. Specifically, note that SmoothAdv [33] can also be viewed as isotropic Gaussian augmentation of ℓ_2 -PGD AT. Importantly, PGD+SNAP achieves a 12% higher $\mathcal{A}_{\text{adv}}^{(U)}$ for the same \mathcal{A}_{nat} . This demonstrates the efficacy of *shaped noise* in SNAP, which enhances the robustness to the union of $(\ell_\infty, \ell_2, \ell_1)$ perturbations.

In order to further quantify importance of *noise shaping*, we also compare ℓ_∞ -PGD+SNAP with ℓ_∞ -PGD+Iso[L], a stronger baseline alternative consisting of *isotropic* Laplace noise augmentation, *i.e.*, *without any noise shaping*. Specifically, in Iso[L], the noise standard deviation is *identical* in each direction, *i.e.*, $\Sigma = \text{Diag} \left[\sqrt{\frac{P_{\text{noise}}}{D}}, \dots, \sqrt{\frac{P_{\text{noise}}}{D}} \right]$. Note that such distributions have recently been explored for RS [43].

Fig. 7(b) plots the \mathcal{A}_{nat} vs. $\mathcal{A}_{\text{adv}}^{(U)}$ trade-off for PGD+SNAP (*red curve*) and PGD+Iso[L] (*black curve*) by sweeping P_{noise} . We find that PGD+SNAP achieves a better \mathcal{A}_{nat} vs. $\mathcal{A}_{\text{adv}}^{(U)}$ trade-off compared to PGD+Iso[L] by making more efficient use of noise power via noise shaping. Specifically, for $\mathcal{A}_{\text{adv}}^{(U)} \approx 38$, PGD+SNAP achieves a $\sim 4\%$ higher \mathcal{A}_{nat} .

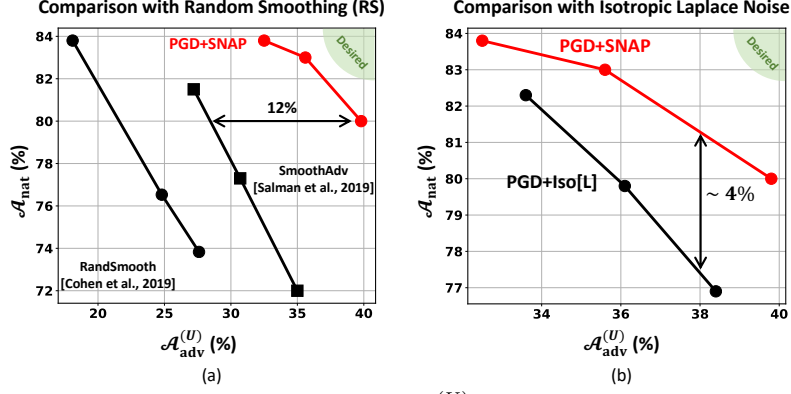


Figure 7: ResNet-18 CIFAR-10 results: (a) \mathcal{A}_{nat} vs. $\mathcal{A}_{\text{adv}}^{(U)}$ for RandSmooth [5], SmoothAdv [33], and PGD+SNAP; (b) \mathcal{A}_{nat} vs. $\mathcal{A}_{\text{adv}}^{(U)}$ for PGD+SNAP and PGD+Iso[L], where Iso[L] denotes a baseline SNAP alternative employing isotropic Laplace noise augmentation, *i.e.*, without noise shaping. PGD+SNAP achieves better \mathcal{A}_{nat} vs. $\mathcal{A}_{\text{adv}}^{(U)}$ trade-off due to noise shaping.

Method	\mathcal{A}_{nat}	$\mathcal{A}_{\text{adv}}^{(\ell_{\infty})}$ $\epsilon = 0.03$	$\mathcal{A}_{\text{adv}}^{(\ell_2)}$ $\epsilon = 0.31$	$\mathcal{A}_{\text{adv}}^{(\ell_1)}$ $\epsilon = 8$	Time per Epoch (seconds)
MNG [21]	79.8	43.9	75.8	53.8	354 [†]
PGD+SNAP	83.1	45.9	74.1	58.3	240

Table 6: ResNet-18 CIFAR-10 results showing a comparison between MNG [21] and PGD+SNAP (from Table 2 in the main text). All MNG numbers are exactly as reported in their paper. We reevaluate PGD+SNAP with our PGD attacks using the new ϵ values used by Madaan et al. [21]. PGD+SNAP achieves 3%, 2%, 4.5% higher \mathcal{A}_{nat} , $\mathcal{A}_{\text{adv}}^{(\ell_{\infty})}$, $\mathcal{A}_{\text{adv}}^{(\ell_1)}$, respectively, while being at least $\sim 40\%$ faster in terms of epoch time. [†]: Note that MNG time is measured on NVIDIA GeForce RTX 2080Ti (by Madaan et al. [21]), while PGD+SNAP is measured on NVIDIA Tesla P100. An RTX 2080Ti has 20% more CUDA cores than a Tesla P100.

B.2 Comparison with Madaan et al. [21]

The meta-noise generator (MNG) [21] employs a multi-layer deep-net to generate noise samples during AT. Importantly, MNG still employs multiple attacks during training, but samples only one of the attacks randomly at a time to reduce the training cost.

However, they have yet to release their code or pretrained models even though their work was posted on arXiv a year ago. Absence of public codes from Madaan et al. [21] makes it difficult to clearly compare with their work, especially in terms of training time. Nonetheless, in this subsection, we try our best to ensure that the comparison is fair. Table 6 reports natural and adversarial accuracy of MNG against $(\ell_{\infty}, \ell_2, \ell_1)$ attacks as reported by Madaan et al. [21]. We find that PGD+SNAP achieves 3%, 2%, 4.5% higher \mathcal{A}_{nat} , $\mathcal{A}_{\text{adv}}^{(\ell_{\infty})}$, and $\mathcal{A}_{\text{adv}}^{(\ell_1)}$, respectively. Note that Madaan et al. [21] evaluate $\mathcal{A}_{\text{adv}}^{(\ell_{\infty})}$ and $\mathcal{A}_{\text{adv}}^{(\ell_2)}$ against PGD-50 attacks, whereas here we employ PGD-100 attacks and, following their protocol, evaluate on the entire CIFAR-10 dataset with a single restart. Furthermore, epoch time for PGD+SNAP is $1.4\times$ smaller than that of MNG [21] even though MNG time was measured on a more recent NVIDIA RTX 2080Ti, which has 20% more CUDA cores than the Tesla P100 GPU that we used for PGD+SNAP.

Importantly, a key advantage of SNAP is its scalability. We are able to report robust ResNet-50 and ResNet-101 networks on ImageNet (Table 4 in the main text), whereas Madaan et al. [21] report results only up to 64×64 TinyImageNet.

Method	\mathcal{A}_{nat}	$\mathcal{A}_{\text{adv}}^{(\ell_\infty)}$ $\epsilon = 0.03$	$\mathcal{A}_{\text{adv}}^{(\ell_2)}$ $\epsilon = 0.5$	$\mathcal{A}_{\text{adv}}^{(\ell_1)}$ $\epsilon = 8$	$\mathcal{A}_{\text{adv}}^{(U)}$
PGD	89.9	45.3	34.9	4.8	4.8
PGD+SNAP	89.3	44.0	67.4	48.3	36.3

Table 7: ResNet-18 SVHN results showing the impact of SNAP augmentation of ℓ_∞ -PGD [22] AT frameworks. Adding SNAP improves $\mathcal{A}_{\text{adv}}^{(U)}$ by $\sim 30\%$ while having only a small impact on \mathcal{A}_{nat} and $\mathcal{A}_{\text{adv}}^{(\ell_\infty)}$.

Method	\mathcal{A}_{nat} (%)
TRADES	81.7
TRADES+SNAP	
$N_0 = 1$	80.1 \pm 0.22
$N_0 = 2$	80.3 \pm 0.14
$N_0 = 4$	80.7 \pm 0.12
$N_0 = 8$	80.9 \pm 0.10
$N_0 = 16$	80.9 \pm 0.08

Table 8: ResNet-18 CIFAR-10 results showing SNAP’s impact on the prediction complexity, where N_0 denotes the number of noise samples employed to estimate $\mathbb{E}[\cdot]$ in Eq. (2) in the main text. We find that for mere accuracy estimation, even a single forward pass ($N_0 = 1$) suffices. $\pm xx$ denotes the standard deviation over 10 independent test runs.

B.3 SVHN results

Table 7 shows PGD and PGD+SNAP results on SVHN data. We train both PGD and PGD+SNAP models for 100 epochs using a piece-wise LR schedule. We start with an initial LR of 0.01 and decay it once at the 95th epoch.

In Table 7, we observe a trend that is similar to our observations for CIFAR-10 and ImageNet results. In particular, for SVHN, SNAP turns out to be even more effective, with $\sim 30\%$ improvement in $\mathcal{A}_{\text{adv}}^{(U)}$ while almost preserving both \mathcal{A}_{nat} and $\mathcal{A}_{\text{adv}}^{(\ell_\infty)}$.

B.4 Impact of SNAP on prediction complexity

While SNAP augmentation has a modest impact on the training time (Table 3 in the main text), here we check whether it could *potentially* increase the model prediction complexity due to the need to estimate the expectation $\mathbb{E}[\cdot]$ in Eq. (2) in the main text.

As expected, by increasing N_0 , the deviation of the \mathcal{A}_{nat} estimate reduces (see Table 8). However, we find that for accuracy estimation, a single forward pass ($N_0 = 1$) suffices. Specifically, an \mathcal{A}_{nat} estimate with $N_0 = 1$ is within 1% of the \mathcal{A}_{nat} estimate with $N_0 = 16$. Furthermore, even with $N_0 = 1$, the standard deviation of \mathcal{A}_{nat} is as low as $\sim 0.2\%$. Thus, the impact of SNAP on prediction complexity can be very small.

B.5 Subspace analysis of adversarial perturbations for TRADES+SNAP model

In this subsection, we carry out a subspace analysis of adversarial perturbations (Section 3 in the main text) for TRADES+SNAP. We confirm that our hypothesis in Section 3 holds even after SNAP augmentation of TRADES. Following the same experimental setup and the notation from Section 3 in the main text, we compute perturbations α_i , β_i , and γ_i for each $x_i \in X$ for ResNet-18 trained using TRADES+SNAP, *i.e.*, $\kappa \equiv \text{rob_sn}$. We compute the singular vector basis \mathcal{P}^κ for the set of ℓ_2 bounded perturbations $\Delta^\kappa = \{\beta_1^\kappa, \dots, \beta_{|X|}^\kappa\}$. Fig. 8 plots the normalized mean squared projections of the three types of perturbation vectors on the singular vector basis \mathcal{P}^κ of a TRADES+SNAP trained ResNet-18. We find that the projections generally follow the same trend as those for a TRADES-trained network which are shown in Fig. 3(b) of the main text. However, we also notice that after SNAP augmentation, the three perturbation types get squeezed into an even smaller 130-dimensional

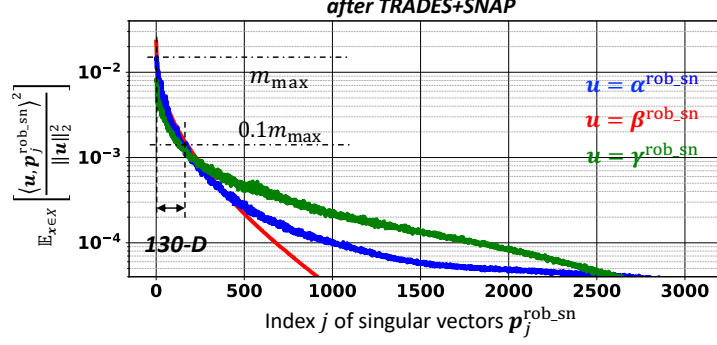


Figure 8: Normalized mean squared projections of three perturbation types on the singular vector basis \mathcal{P}^κ of ℓ_2 perturbations of ResNet18 on CIFAR-10 after TRADES+SNAP training ($\kappa \equiv \text{rob_sn}$). The singular vectors \mathbf{p}_i^κ comprising $\mathcal{P}^\kappa = \{\mathbf{p}_1^\kappa, \dots, \mathbf{p}_D^\kappa\}$ are ordered in descending order of their singular values.

Method	\mathcal{A}_{nat}	$\mathcal{A}_{\text{adv}}^{(\ell_\infty)}$ $\epsilon = 0.03$	$\mathcal{A}_{\text{adv}}^{(\ell_2)}$ $\epsilon = 0.5$	$\mathcal{A}_{\text{adv}}^{(\ell_1)}$ $\epsilon = 12$	$\mathcal{A}_{\text{adv}}^{(U)}$
PGD	84.6	48.8	62.3	15.0	15.0
Noise shaping basis $V = \mathbf{I}_{D \times D}$					
+SNAP[G]	80.7	45.7	66.9	34.6	31.9
+SNAP[U]	85.1	42.7	66.7	28.6	26.6
+SNAP[L]	83.0	44.8	68.6	40.1	35.6
Noise shaping basis $V = U_{\text{img}}$					
+SNAP[G]	81.7	48.9	67.5	29.8	28.7
+SNAP[U]	82.0	46.6	67.8	27.8	25.7
+SNAP[L]	81.7	46.8	65.9	28.5	27.4

Table 9: ResNet-18 CIFAR-10 results showing the impact of noise shaping basis V for ℓ_∞ -PGD [22] AT framework with SNAP. In this table, SNAP[G], SNAP[U], and SNAP[L] denote shaped noise augmentations with Gaussian, Uniform, and Laplace noise distributions, respectively, and U_{img} refers to the singular vector basis of the training images.

subspace, *i.e.*, projections are $< 10\%$ of the maximum projection value for all dimensions beyond the first 130 dimensions.

B.6 Impact of noise shaping in the image basis

Recall that, for all experiments in the main text, we chose the noise shaping basis $V = \mathbf{I}_{D \times D}$, *i.e.*, the noise was shaped and added in the standard basis in \mathbb{R}^D , where $\mathbf{I}_{D \times D}$ denotes the identity matrix (see Eq. (1) and Alg. 1 in the main text).

In this section, we explore the shaped noise augmentation in the *image basis*, *i.e.*, singular vector basis of the training set images. Specifically, we choose $V = U_{\text{img}} = [\mathbf{u}_1, \dots, \mathbf{u}_D]$, where U_{img} denotes the singular vector basis of the images in the training set. Thus, the sampled noise vector \mathbf{n}_0 (see Eq. (1) in the main text) is scaled by direction-wise standard deviation matrix Σ and *rotated* by U_{img} before being added to the input image \mathbf{x} .

The rationale for choosing $V = U_{\text{img}}$ is as follows: Recent works [15, 35, 34] have demonstrated the generative behavior of adversarial perturbations of networks trained with single-attack AT, *i.e.*, adversarial perturbations of robust networks exhibit semantics similar to the input images. Thus, the perturbation basis (see section 3 in the main text) of the robust networks trained with single-attack AT seems to be aligned with the image basis.

We repeat the experiments in Table 1 of the main text while keeping all the settings *identical* except for choosing $V = U_{\text{img}}$ instead of $V = \mathbf{I}_{D \times D}$. Table 9 shows the results. The first three rows

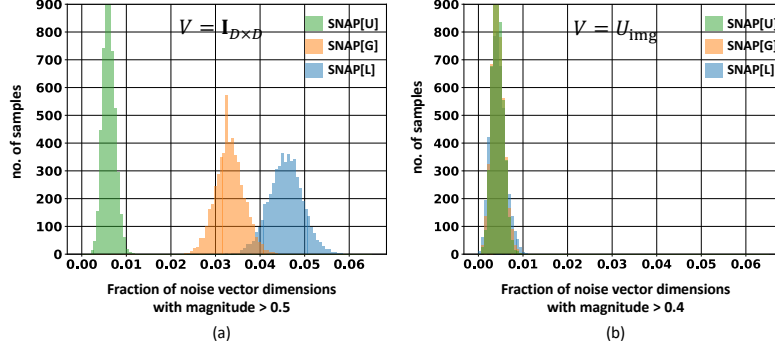


Figure 9: ResNet18 CIFAR-10 results: histograms of the fraction of noise vector dimensions with magnitude (a) > 0.5 when $V = \mathbf{I}_{D \times D}$, and (b) > 0.4 when $V = U_{\text{img}}$. Histograms are plotted for 5000 random noise samples \mathbf{n} . The three shaped noise distributions are from the corresponding networks in Table 9.

correspond to $V = \mathbf{I}_{D \times D}$ and are reproduced from Table 1 of the main text. Note that, in order to preserve $\mathcal{A}_{\text{nat}} > 81\%$, we need to reduce $P_{\text{noise}} = 60$ when $V = U_{\text{img}}$, since the noise is now pixel-wise correlated.

In Table 9, we notice that $\mathcal{A}_{\text{adv}}^{(\ell_1)}$ is significantly reduced when $V = U_{\text{img}}$ as compared to the case $V = \mathbf{I}_{D \times D}$. More interestingly, all three types of noise distributions result in similar values for $\mathcal{A}_{\text{adv}}^{(\ell_1)}$ when $V = U_{\text{img}}$. We discuss this phenomenon in the next section, *i.e.*, Sec. B.7 below.

Table 9 shows that the orientation of a noise vector is as important as its distribution. The simpler choice of $V = \mathbf{I}_{D \times D}$ turns out to be more effective.

B.7 Understanding the effectiveness of SNAP[L] for ℓ_∞ AT

In this subsection, we conduct additional studies to further understand the following two observations in SNAP: (i) shaped Laplace noise is particularly effective (Table 1 in the main text), and (ii) rotating noise vectors ($V = U_{\text{img}}$) reduces their effectiveness (Table 9 in this Supplementary). We study the properties of the noise vector \mathbf{n} for different noise distributions.

We conjecture that the Laplace distribution is most effective because of its heavier tail compared to Gaussian and Uniform distributions of the same variance. A long-tailed distribution will generate more large magnitude elements in a vector drawn from it and hence is more effective in emulating a strong ℓ_1 -norm bounded perturbation. Furthermore, the standard (un-rotated) basis preserves this unique attribute of samples drawn from such distributions.

This conjecture is validated by Fig. 9(a) which shows that noise samples drawn from the Laplace distribution in the standard basis have the highest average number of dimensions with large (> 0.5) magnitudes, followed by Gaussian and Uniform distributions. This correlates well with the results in Table 1 in the main text and Table III (first three rows), in that $\mathcal{A}_{\text{adv}}^{(\ell_1)}$ is the highest for Laplace followed by those for Gaussian and Uniform. Additionally, the use of $V = U_{\text{img}}$ dissolves this distinction between the three distributions as shown in Fig. 9(b) which explains the similar (and lower) $\mathcal{A}_{\text{adv}}^{(\ell_1)}$ values for all three distributions in Table III.

Thus, we confirm that the type of noise plays an important role in robustifying single-attack ℓ_∞ AT frameworks to the union of multiple perturbation models. Specifically, the noise vectors with higher fraction of noise dimensions with larger magnitudes are better at complementing ℓ_∞ AT frameworks.

B.8 Evaluating common corruptions and functional attack

In this subsection, we check if there are any other downsides of SNAP when it improves robustness against the union of $(\ell_\infty, \ell_2, \ell_1)$ perturbations. In particular, we check if SNAP improvements are achieved at the cost of a drop in accuracy against common corruptions [13] or functional adversarial attacks [18].

Method	\mathcal{A}_{nat}	$\mathcal{A}_{\text{adv}}^{(U)}$	\mathcal{A}_{cc}	$\mathcal{A}_{\text{adv}}^{(f)}$ ReColorAdv
Vanilla	94.5	0.0	72.0	0.9
ℓ_∞ -PGD	84.6	15.0	75.6	53.5
Noise shaping basis $V = \mathbf{I}_{D \times D}$				
+SNAP[G]	80.7	31.9	72.8	55.1
+SNAP[U]	85.1	26.6	75.0	46.9
+SNAP[L]	83.0	35.6	75.3	51.3
Noise shaping basis $V = U_{\text{img}}$				
+SNAP[G]	81.7	28.7	73.6	54.5
+SNAP[U]	82.0	25.7	73.1	54.0
+SNAP[L]	81.7	27.4	73.4	55.3

Table 10: ResNet-18 CIFAR-10 results showing natural accuracy \mathcal{A}_{nat} , adversarial accuracy $\mathcal{A}_{\text{adv}}^{(U)}$ against the union of $(\ell_\infty, \ell_2, \ell_1)$ perturbations, accuracy \mathcal{A}_{cc} in the presence of common corruptions [13], and adversarial accuracy $\mathcal{A}_{\text{adv}}^{(f)}$ against a functional adversarial attack ReColorAdv [18]. All accuracy numbers are in %. In this table, $\mathbf{I}_{D \times D}$ denotes D -dimensional identity matrix, while U_{img} denotes singular vector basis of the training images. We find that SNAP augmentations of ℓ_∞ -PGD significantly ($\approx 20\%$) improve $\mathcal{A}_{\text{adv}}^{(U)}$ while preserving both \mathcal{A}_{cc} and $\mathcal{A}_{\text{adv}}^{(f)}$.

We use corrupted images provided by Hendrycks & Dietterich [13] to estimate accuracy in the presence of common corruptions (\mathcal{A}_{cc}). We average the accuracy numbers across different corruption strengths and types. Also, we use the ReColorAdv setup of Laidlaw et al. [19] to estimate accuracy against functional adversarial attacks ($\mathcal{A}_{\text{adv}}^{(f)}$). We also make it *adaptive* to our defense framework via appropriate noise averaging (similar to our adaptive PGD attacks [33] discussed in the main text) to eliminate any gradient obfuscations. As observed in Table 10, SNAP augmentations of PGD AT generally preserve both \mathcal{A}_{cc} and $\mathcal{A}_{\text{adv}}^{(f)}$. In particular, 20.6% improvement in $\mathcal{A}_{\text{adv}}^{(U)}$ via PGD+SNAP[L] (with $V = \mathbf{I}_{D \times D}$) is accompanied with the same \mathcal{A}_{cc} and only a 2.2% lower $\mathcal{A}_{\text{adv}}^{(f)}$ ($= 51.3\%$) compared to PGD AT. In contrast, vanilla training achieves an $\mathcal{A}_{\text{adv}}^{(f)}$ of only 0.9%. Even with $V = U_{\text{img}}$, PGD+SNAP[L] achieves a 1.8% higher $\mathcal{A}_{\text{adv}}^{(f)}$ along with a 12.4% improvement in $\mathcal{A}_{\text{adv}}^{(U)}$. Note that all $\mathcal{A}_{\text{adv}}^{(U)}$ numbers are identical to the ones reported in Sec. B.6.

We conclude that SNAP augmentation of PGD AT improves $\mathcal{A}_{\text{adv}}^{(U)}$ by up to 20% while preserving its robustness against common corruptions and functional adversarial attacks. Thus, SNAP expands the capabilities of ℓ_∞ AT frameworks without any significant downside. However, further work is required to improve robustness to a larger class adversarial attacks, such as rotation [7], texture [2], etc., simultaneously.

B.9 Error bars

In this subsection, we confirm that benefits of SNAP are not specific to any particular choice of random seed. Specifically, we run both PGD+SNAP (with superconvergence) and FreeAdv+SNAP (see Table 3 in the main text) training four times with different random seeds. Table 11 shows the mean accuracy and its standard deviation for each of \mathcal{A}_{nat} , $\mathcal{A}_{\text{adv}}^{(\ell_\infty)}$, $\mathcal{A}_{\text{adv}}^{(\ell_2)}$, $\mathcal{A}_{\text{adv}}^{(\ell_1)}$, and $\mathcal{A}_{\text{adv}}^{(U)}$ with ResNet-18 on CIFAR-10. We find that the standard deviation of accuracy is $\approx 0.5\%$ in almost all cases. This demonstrates the ease of replicating SNAP results.

Appendix C Additional Details

C.1 Details of Hyperparameters

C.1.1 Attack hyperparameters

As mentioned in the main text, we follow basic PGD attack formulations of Maini et al. [23]. We further enhance them to target the full defense – SN layer – since SNAPnet is end-to-end differentiable. Specifically, we backpropagate to the primary input x through the SN layer (see Fig. 4(b) in the

Method	\mathcal{A}_{nat}	$\mathcal{A}_{\text{adv}}^{(\ell_\infty)}$ $\epsilon = 0.03$	$\mathcal{A}_{\text{adv}}^{(\ell_2)}$ $\epsilon = 0.5$	$\mathcal{A}_{\text{adv}}^{(\ell_1)}$ $\epsilon = 12$	$\mathcal{A}_{\text{adv}}^{(U)}$
PGD+SNAP	82.5 \pm 0.27	43.1 \pm 0.61	66.9 \pm 0.57	39.0 \pm 0.41	33.7 \pm 0.29
FreeAdv+SNAP	83.4 \pm 0.25	39.2 \pm 0.74	65.7 \pm 0.55	36.5 \pm 0.60	30.4 \pm 0.83

Table 11: ResNet-18 CIFAR-10 results showing the mean and standard deviation for all accuracies over four different training runs of PGD+SNAP (with superconvergence) and FreeAdv+SNAP. As observed, the standard deviation in accuracy is $\approx 0.5\%$ in almost all cases, demonstrating the ease of replicating SNAP results.

main text). Thus, the final shaped noise distribution is exposed to the adversary. We also account for the $\mathbb{E}_{\mathbf{n}}[\cdot]$ (see Eq. (2) in the main text) by explicitly averaging deep net logits over N_0 noise samples *before* computing the gradient, which eliminates any gradient obfuscation, and was shown to be the strongest attack against noise augmented models [33]. We choose $N_0 = 8$ for all our attack evaluations.

For ℓ_2 and ℓ_∞ PGD attacks, we choose steps size $\alpha = 0.1\epsilon$. For ℓ_1 PGD attacks, we choose the exact same configuration as Maini et al. [23].

C.1.2 Training hyperparameters

As mentioned in the main text, we introduce SNAP without changing any hyperparameters of BASE() AT. All BASE() and BASE()+SNAP training runs on CIFAR-10 employ an SGD optimizer with a fixed momentum of 0.9, batch size of 250, and weight decay of 2×10^{-4} . Also, while accounting for the $\mathbb{E}_{\mathbf{n}}[\cdot]$ (see Eq. (2) in the main text), note that $N_0 = 1$ suffices during BASE()+SNAP training. Below we provide specific details for each SOTA AT framework:

BASE() \equiv PGD [22] on CIFAR-10:

ℓ_∞ -PGD AT employed ℓ_∞ -bounded PGD- K attack with $\epsilon = 0.031$, step size $\alpha = 0.008$, and $K = 10$. For ℓ_2 -PGD AT, we used an ℓ_2 -bounded PGD- K attack with $\epsilon = 0.5$, step size $\alpha = 0.125$ and $K = 10$. Following Rice et al. [30], we employed 100 epochs for PGD AT with step learning rate (LR) schedule, where LR was decayed from 0.1 to 0.01 at epoch 96. Following Maini et al. [23], we also employed *their* cyclic LR schedule to achieve superconvergence in 50 epochs. Following Maini et al. [23], we set weight decay to 5×10^{-4} in PGD AT.

In PGD+SNAP, the noise variances were updated every $U_f = 10$ epochs and we use $P_{\text{noise}} = 160$ in Tables 1, 2, and 3 in the main text.

BASE() \equiv TRADES [46] on CIFAR-10:

Following Zhang et al. [46], TRADES AT employed ℓ_∞ -bounded perturbations with $\epsilon = 0.031$, step size $\alpha = 0.007$, and attack steps $K = 10$. We set TRADES parameter $1/\lambda = 5$, which controls the weighing of its robustness regularizer. It was trained for 100 epochs with a step LR schedule, where LR was decayed to $\{0.01, 0.001, 0.0001\}$ at the epochs $\{75, 90, 100\}$, respectively. Following Maini et al. [23], we also employed *their* cyclic LR schedule to achieve superconvergence in 50 epochs, while keeping all other settings identical.

In TRADES+SNAP, the noise variances were updated every $U_f = 10$ epochs and we use $P_{\text{noise}} = 120$ in Tables 2 and 3 in the main text.

BASE() \equiv FreeAdv [35] on CIFAR-10:

Following Shafahi et al. [35], FreeAdv AT was trained for 25 epochs, each consisting of a replay of 8. It employed ℓ_∞ perturbations with $\epsilon = 0.031$. The learning rate was decayed to $\{0.01, 0.001, 0.0001\}$ at epochs $\{13, 19, 23\}$, respectively.

In FreeAdv+SNAP, the noise variances were updated every $U_f = 5$ epochs, since the replay of 8 scales down the total number of epochs. Also, we use $P_{\text{noise}} = 160$ in Tables 2 and 3 in the main text.

BASE() \equiv FastAdv [40] on CIFAR-10:

Following Wong et al. [40], FastAdv AT employed a single-step ℓ_∞ norm bounded FGSM attack with $\epsilon = 8/255$, step size $\alpha = 10/255$, and random noise initialization. It was trained for 50 epochs with the *same* cyclic LR schedule used by Wong et al. [40]. We used a weight decay of 5×10^{-4} .

In FastAdv+SNAP, the noise variances were updated every $U_f = 10$ epochs and we use $P_{\text{noise}} = 200$ in Tables 2 and 3 in the main text.

BASE() \equiv FreeAdv [35] on ImageNet:

Following Shafahi et al. [35], FreeAdv AT was trained for 25 epochs, each consisting of a replay of 4. It employed ℓ_∞ perturbations with $\epsilon = 4/255$, *identical* to the authors' original setup. The LR was decayed by 0.1 every 8 epochs, starting with the initial LR of 0.1. We used weight decay of 1×10^{-4} .

In FreeAdv+SNAP, the noise variances were updated every $U_f = 5$ epochs, since the replay of 4 scales down the total number of epochs. Also, we use $P_{\text{noise}} = 4500$ in Table 4 in the main text, which corresponds to noise standard deviation of ~ 0.17 per pixel *on average*.

MSD- K [23] experiments for $K \in \{30, 20, 10, 5\}$:

Maini et al. [23] report results for only MSD-50 in their paper. We produce MSD- K results using their publicly available code. While reducing the number of steps in MSD, we *appropriately* increase the step size α for the attack. For MSD-50, Maini et al. [23] used $\alpha = (0.003, 0.05, 1.0)$ for $(\ell_\infty, \ell_2, \ell_1)$ perturbations, respectively. We proportionately increase the step size to $\alpha = (0.005, 0.084, 1.68)$ and $\alpha = (0.0075, 0.125, 2.5)$ for MSD-30 and MSD-20, respectively.

For MSD-10 and MSD-5, we choose $\alpha = (0.0075, 0.125, 2.5)$, since we found that further increasing the step size α lead to *lower* final adversarial accuracy.

Other than the step-size, we do *not* make any change to the original code by Maini et al. [23].

AVG- K [37] experiments for $K \in \{30, 20, 10, 5\}$:

For AVG-50, we use the publicly available model provided by Maini et al. [23]. We produce AVG- K results using the Maini et al. [23] code. When reducing the number of steps, we appropriately increase the step size α for ℓ_∞ and ℓ_2 perturbations. Increasing the step size for ℓ_1 perturbations resulted in significantly lower $\mathcal{A}_{\text{adv}}^{(U)}$, and thus α for ℓ_1 perturbations was kept constant while reducing the number of steps. For AVG-50, Maini et al. [23] used $\alpha = (0.003, 0.05, 1.0)$ for $(\ell_\infty, \ell_2, \ell_1)$ perturbations, respectively. We increase the ℓ_∞ and ℓ_2 step sizes to set $\alpha = (0.005, 0.084, 1.0)$ and $\alpha = (0.0075, 0.125, 1.0)$ for AVG-30 and AVG-20 respectively.

As with MSD, we do not further increase the step size α for AVG-10, AVG-5, and instead choose $\alpha = (0.0075, 0.125, 1.0)$. Even here, we found that increasing the step size for ℓ_1 perturbations results in lower $\mathcal{A}_{\text{adv}}^{(U)}$. For AVG-2, we increase the step size for all perturbations to $\alpha = (0.024, 0.4, 8)$.

PAT [19] on CIFAR-10:

For comparisons with Laidlaw et al. [19], we evaluate their publicly available self-bounded ResNet-50 model.

C.2 Details about SNAP

C.2.1 Distribution Update Epoch

In the SNAP distribution update epoch (see Algorithm 1 in the main text), we employ ℓ_2 norm-bounded PGD attack to compute perturbation vectors $\boldsymbol{\eta}$. We use only 20% of the training data, which is randomly selected during every SNAP update epoch. Recall that normalized root mean squared projections of $\boldsymbol{\eta}$ dictate the updated noise variances (Eq. (3) in the main text). In the following we provide more details specific to CIFAR-10 and ImageNet data:

CIFAR-10: we employ 10 step ℓ_2 -PGD attack with $\epsilon = 1.8$ and $N_0 = 4$.

ImageNet: we employ 4 step ℓ_2 -PGD attack with $\epsilon = 4.0$ and $N_0 = 1$.

Note that ℓ_2 norm bound ϵ for the PGD attack here does not play any role, since $\boldsymbol{\eta}$ perturbation projections are normalized.

C.2.2 Noise variance initialization in SNAP

In SNAP, we initialize the noise variances to be uniform across all dimensions. Specifically, in Algorithm 1 in the main text, $\Sigma_0 = \text{Diag} \left[\sqrt{\frac{P_{\text{noise}}}{D}}, \dots, \sqrt{\frac{P_{\text{noise}}}{D}} \right]$ for a given value of P_{noise} .

Appendix D Accompanying Code and Pretrained Models

As a part of this appendix, we share our code to reproduce PGD+SNAP and TRADES+SNAP results on CIFAR-10 (Table 2 in the main text) and FreeAdv+SNAP results on ImageNet (Table 4 in the main text). We also share corresponding pretrained models to facilitate quick reproduction of our results. Code and models are available at link: <https://github.com/adpatil2/SNAP>